On the feasibility of dynamic substructuring for hybrid testing of vibrating structures

An Hu[*]
School of Engineering
University of Liverpool
Liverpool, UK L69 3GH
Email: huanstudent@gmail.com

Paolo Paoletti
School of Engineering
University of Liverpool
Liverpool, UK L69 3GH
Email: P.Paoletti@liverpool.ac.uk

ABSTRACT

Dynamically substructured systems (DSS) are a typical technique to achieve real-time numerical simulations combined with physically tested components. However, a rigorous feasibility analysis before the implementation is missing. This paper is aimed to fill this gap by establishing rigorous conditions for when DSS is suitable for dynamic testing. The proposed method is based on novel symbolic recursive formulations for the transfer functions describing a generic lumped parameter vibrating structure, enabling the analysis of structural and other properties without requiring the computation of explicit symbolic expressions for the transfer functions involved, representing a significant breakthrough as it allows to perform feasibility analysis in analytical form, rather than solely relying on numerical approaches. The series of analytical conclusions presented in this paper, and future ones unlocked by the proposed approach, will significantly enrich the research in the community of DSS and structural vibrations. In particular, the proposed approach allows performing analysis of causality, controllability and observability using much reduced knowledge of the structure, thus significantly simplifying such analysis. Analytical conclusions on stability can also be made with the help of novel recursive form, removing the need of repeatedly calculating the roots of characteristic equations, a task that can be performed only via numerical approaches and for which analytical results are not available. The

---

[*]Address all correspondence for other issues to this author.

proposed methodology can be applied to a whole class of vibration problems and is not linked to any specific structure, going beyond the specific examples available in the literature.

Keywords : dynamically substructured systems, hybrid testing, structural vibrations causality, controllability and observability.

1   Introduction

Experimental testing of large, nonlinear or complex structures can be very expensive and time consuming. To alleviate these issues, several techniques have been proposed in the literature to replace part of the structure by a numerical simulator and then design a control system so that the combination of numerical and physical subsystems exhibits the same dynamical response of the original structure.

Dynamically Substructured Systems (DSS) are part of this family of techniques,alongside similar approaches also known as hybrid testing, hybrid simulation or real time hybrid simulation (RTHS) [1–3]. In this paper we focus on the DSS framework shown in Figure 1, where the original structure is decomposed into two main parts, the physical part and the numerical part. The numerical part simulates a subsystem of the original structure. On the other hand, the physical part is composed of a physical structure and of an actuator which is used to simulate the presence of the subsystem that has been replaced by the numerical part. The challenge is then to control the actuator at the interface so that the closed loop behaviour of the DSS emulates the dynamic behaviour of the complete original structure [4, 5].
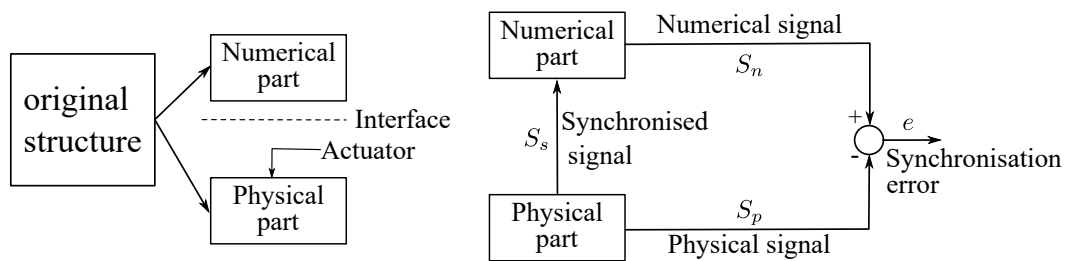

Fig. 1.   DSS schematic: the original structure is split into a numerical part and a physical part. The synchronisation signal $S_s(t)$ is measured on the physical part and transmitted as input to the numerically simulated subsystem. The goal of a DSS controller to control the actuator at the interface with the goal of minimising the error $e(t)$ between the numerical response S_n and the physical signal S_p so that the overall behaviour of the DSS is the same of the original structure.

Two main approaches have been proposed in the literature to tackle this challenge: force control and position control. In the force control setting, the displacement of the physical part at the interface (indicated by *synchronised signal S_s* in Figure 1) is measured and transmitted as an input to the numer-

ical part. The simulator used in the numerical part then calculates the force at the interface (*numerical signal S_n*) which is compared with the force generated by the actuator situated at the corresponding interface in the physical part (*physical signal S_p*). A feedback controller is then designed to minimise the *synchronisation error e* between the simulated force and the actuator force, so that the interface becomes transparent and the DSS behaves as the original structure. In the displacement control setting, the role of force and displacement is swapped. The interested reader is referred to the review paper by Klerk *et al.* [5] for an extensive review of DSS approaches.

The presence of delays, disturbances and model uncertainties prevents exact cancellation of the error between numerical and physical signals, therefore a feedback controller is needed to control the actuator in order to minimise the synchronisation error. Typical linear feedback controller design techniques used for such purpose include linear substructing control (LSC) and minimal control with error feedback (MCEF) [6]. Robustness of these techniques has been thoroughly studied, see for example the results by Gawthrop [7] and Tu [8]. Traditional control strategies - such as H_∞ [9], control sliding mode [10] and real-time model updating [11] - have also been applied to nonlinear or uncertain DSS problems. Similarly, delay compensation techniques have been proposed to minimise the detrimental effects of delays introduced by the control logic [12–14], as well as the efforts trying to predict and compensate delays with generalised methodologies[15, 16]. Nonlinear substructuring control (NLSC) was also proposed as an extension to traditional LSC to deal with nonlinear dynamic problems [17]. Issues related to application of hybrid testing to systems exhibiting chaotic behaviours, such as a nonlinear pendulum model, have also been analysed in [18].

These control strategies have been successfully used to test dynamical systems across different domains. For example, in the railway industry Stoten and colleagues tested a pantograph using a DSS approach where only the pantograph was physical, whereas the electric line was simulated [19]. Similarly, Facchinetti used DSS to study the pantograph-catenary interaction [20], whereas Hong used DSS to analyse the characterisation of rail tracks [21]. Allen exploited DSS to aid the design of NASA rocket launcher [22] and Mayes developed the applications of DSS to transmission structures, which is helpful for experiments on rotational structures such as wind turbines [23]. In addition, the DSS approach can be applied to vehicle development as well; for example van der Seijs and Rixen proposed proposed a DSS framework for a variety of experiments on vehicle structures [24]. Similarly, models of motorcycles have been tested using DSS techniques [4, 25]. Dynamic substructuring is also widely used in civil and structural engineering to test, for example, nonlinear components [26–28], seismic responses [29–31], piping systems [32] and soil-structure interaction [33]. A review of dynamic substructuring techniques

can be found, for example, in the review paper by Klerk *et al.* [5].

Although DSS and the relative common techniques has been extensively studied for different applications, one of the common issues which should not be neglected and could seriously jeopardise future studies is the excessive focus on specific models. Indeed, most of the available literature has been focused on specific benchmark systems or on specific examples. Systems with only two or three degrees of freedom were typically selected for analyses, thus posing the fundamental questions of, for example, whether the conclusions can be expanded to systems with different degrees of freedom and whether and how the system parameters affect the conclusions. Without clearly addressing these issues, most of the conclusions reported in the literature can only be regarded as the summaries for those specific models. The path to generalisation to other models and application is therefore unclear, a factor that can severely limit the applications and future studies of DSS. Another gap in the current literature is the lack of a comprehensive feasibility analysis, with only limited exceptions such as the recent paper by Terkovics *et al.* [34] where the effect of the interface location on DSS performance was studied, as well as the paper by Gawthrop *et al.* [35] where the causality analysis for DSS was studied. However, both studies still focused on specific models only, meaning a comprehensive analysis of generic structural properties affecting feasibility of DSS design is lacking in the available literature. Even before starting the control design process for a given DSS decomposition, one needs to know if a controller can be designed in the first place, and this feasibility analysis is missing for generic structures in the literature.

In this paper an approach to fill this gap is proposed. Two main contributions are made in this paper. The first one is the derivation of a novel recursive formulation to derive transfer functions for lumped parameter systems composed of a chain of mass-spring-damper systems, which allows a greatly simplified analysis of structural properties of lumped parameter DSS, irrespective of the number of degrees of freedom and specific values of system parameters. The benefits of the proposed formulation include, but are not limited to, analytical conclusions on stability analysis for similar structures with different degrees of freedom [36], which are impossible to be drawn by using numerical methodologies. This is a significant advancement compared to the traditional approach solely relying on numerical analyses in DSS and vibration communities, with more analytical conclusions being possible to be found in future to further enrich the achievements. Although a mass-spring-damper chain is selected for demonstration and the results presented might only be suitable for this class of systems, this class already describes a wide range of vibration models [25, 34] considered by the vibration community. This is the first step towards a more generalised analysis framework of DSS properties for generic vibrating structures. Moreover, given the structural similarities of equations of motion for lumped parameter systems, the

proposed formulation can be expanded to different types of structures, which can significantly broaden the applications of DSS. The methodology proposed in this paper also enable several analytical results on feasibility of DSS decomposition for *generic* vibrating structures, the second major contribution of this paper. For example, it allows assessing whether a given DSS decomposition and control strategy can be designed for a *generic* lumped parameter vibration system with n degrees of freedom. This, in turns, allows the proposal of general guidelines regarding the type of DSS decomposition and actuator/sensor arrangements to be used in any particular real world application. The focus here is on structural properties and the scope of this paper does not include implementation details - such as the delays imposed by the electronics used to implement the controller and the potential effects of the actuator dynamics - that may hinder the main message of this paper. Extensions to cover these aspects can be easily obtained by, for example, including the terms related to delays and actuator transfer functions in the proposed methodology, as briefly mentioned throughout the paper.

The problem analysed in this manuscript is formally stated in Section 2 for a widely used class of benchmark systems, together with a brief review of the main concepts of structural stability, controllability, causality and observability that will be used for the analysis presented in this paper. A causality study to obtain feasible DSS configurations is reported in Section 4 and provides constraints on the choice of using either directly measured or indirectly estimated synchronised signals for control purposes. The identified causal configurations are then further analysed in Section 5 to assess their structural properties of observability and controllability, and hence assess if a synchronising controller can be designed. The proposed methodology is applicable to any DSS design for vibrating structures, and hence is not linked to any physical or experimental realisation of such class of structures. However, for the sake of completeness, numerical examples are briefly discussed in Section 6 to show how the outcomes of the analyses in Section 4 and Section 5 may inform control design for real applications. These include a complex frame structure which does not fall within the class of benchmark systems used to motivate most of the analysis, but for which strucutural analogies with the class of system used through the paper can be used to successfully infer DSS feasibility. Finally, some concluding remarks and suggestions for future research directions are reported in Section 7.

2 Problem statement and methodology

This paper initially focuses on a generic class of lumped parameter vibration models, which can be schematically represented as chain of n spring-damper-mass systems, as shown in Figure 2. As mentioned earlier, although the results presented in this paper strictly apply only to this class of systems,

the final results may still be exploited by considering structural similarities with the equations of motions of more generic vibratory systems. An example of such extension is presented in Section 6.2. In our framework, a disturbance $d(t)$ is applied as displacement of the support at one end of the structure, whereas an external force $F(t)$ may be applied to the other end (such force will represent, for example, the action of the actuator used in DSS substructuring in the following sections of the paper).
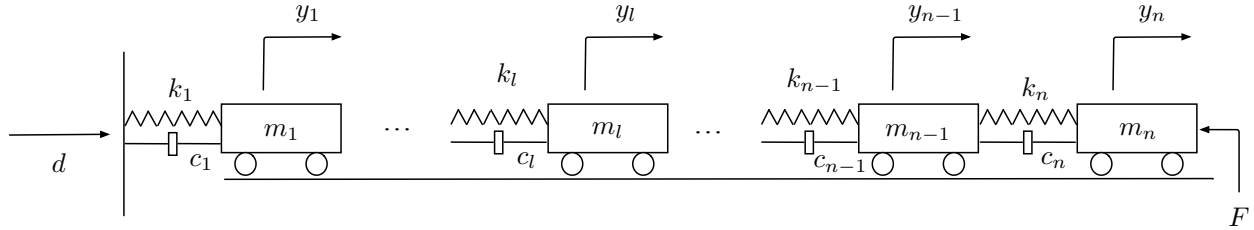

Fig. 2. Schematic representation of the benchmark system considered initially in this paper.

2.1 Original dynamics

The equations of motion describing the behaviour of the structure in Figure 2 (sometime referred to as *emulated system* in the DSS literature [4]) can be obtained by imposing force balance at each mass and read

$$
\begin{cases}
m_n \ddot{y}_n = -k_n(y_n - y_{n-1}) - c_n(\dot{y}_n - \dot{y}_{n-1}) - F \\
\quad \vdots \\
m_i \ddot{y}_i = -k_i(y_i - y_{i-1}) - c_i(\dot{y}_i - \dot{y}_{i-1}) + k_{i+1}(y_{i+1} - y_i) + c_{i+1}(\dot{y}_{i+1} - \dot{y}_i) \\
\quad \vdots \\
m_1 \ddot{y}_1 = -k_1(y_1 - d) - c_1(\dot{y}_1 - \dot{d}) + k_2(y_2 - y_1) + c_2(\dot{y}_2 - \dot{y}_1)
\end{cases}
\tag{1}
$$

where m_i is the i-th mass, c_i is the i-th damping coefficient, k_i is the i-th spring stiffness, y_i is the displacement of the i-th mass and the dot indicates time derivative. The displacement of the support is indicated as $y_0 = d$ and is considered unknown. An equivalent expression in the frequency domain can then be written as

$$Y_i(s) = \frac{Num_i(s)}{Den_i(s)} Y_{i-1}(s) - \frac{Num1_i(s)}{Den1_i(s)} F(s) \tag{2}$$

where $Num_i(s)$ and $Den_i(s)$ represent, respectively, the numerator and the denominator of the transfer function between the position of the i-th and $(i-1)$-th masses. Similarly $Num1_i(s)$ and $Den1_i(s)$ refer to the transfer function between the position of the i-th mass and the applied force F.

The linearity of the system dynamics (1)-(2) implies that the superposition principle holds, hence the influence of the disturbance d and the force F can be assessed independently. For example, the transfer function between i-th mass displacement y_i and the disturbance d can be written as

$$\frac{Y_i(s)}{d(s)} = \frac{Y_1(s)}{d(s)} \frac{Y_2(s)}{Y_1(s)} \cdots \frac{Y_i(s)}{Y_{i-1}(s)} = \frac{Num_i^d}{Den_1} = \begin{cases} \dfrac{Den_{i+1} \prod_1^i (c_i s + k_i)}{Den_1} & i \leq n-1 \\[3mm] \dfrac{\prod_1^i (c_i s + k_i)}{Den_1} & i = n \end{cases} \tag{3}$$

where

$$Den_n = m_n s^2 + c_n s + k_n$$

$$Den_{n-1} = [m_{n-1}s^2 + (c_{n-1} + c_n)s + k_{n-1} + k_n](m_n s^2 + c_n s + k_n) - (c_n s + k_n)^2$$

$$Den_i = [m_i s^2 + (c_i + c_{i+1})s + k_i + k_{i+1}]Den_{i+1} - (c_{i+1}s + k_{i+1})^2 Den_{i+2} \tag{4}$$

A similar procedure can also be applied to derive the transfer function between the i-th displacements y_i and the external force F, thus obtaining

$$\frac{Y_i(s)}{F(s)} = \frac{Y_n(s)}{F(s)} \frac{Y_{n-1}(s)}{Y_n(s)} \cdots \frac{Y_i(s)}{Y_{i+1}(s)} = -\frac{Num_i^F}{Den1_n} = \begin{cases} -\dfrac{\prod_{i=2}^n (c_i s + k_i)}{Den1_n} & i = 1 \\[3mm] -\dfrac{Den1_{i-1} \prod_{i+1}^n (c_{i+1}s + k_{i+1})}{Den1_n} & 1 < i \leq n-1 \\[3mm] -\dfrac{Den1_{i-1}}{Den1_n} & i = n \end{cases} \tag{5}$$

where

$$Den1_i = \begin{cases} m_1 s^2 + (c_1 + c_2)s + k_1 + k_2 & i = 1 \\ [m_1 s^2 + (c_1 + c_2)s + k_1 + k_2][m_2 s^2 + (c_2 + c_3)s + k_2 + k_3] - (c_2 s + k_2)^2 & i = 2 \\ [m_i s^2 + (c_i + c_{i+1})s + k_i + k_{i+1}]Den1_{i-1} - (c_i s + k_i)^2 Den1_{i-2} & 2 < i \leq n-1 \\ (m_n s^2 + c_n s + k_n)Den1_{n-1} - (c_n s + k_n)^2 Den1_{n-2} & i = n \end{cases} \tag{6}$$

Note that $Den1_n$ is equal to Den_1, as they both are the characteristic equations of the system. The degrees of the numerators and the denominators are summarised in Table 1 for reference.

The recursive expressions derived in (3) and (5), and the associated Table 1, will play a key role in the subsequent analysis, as they allow the assessment of causality and structural properties without requiring detailed knowledge of the structure parameters. Here, a dynamical system is called *causal* if its response depends only on past and current inputs [37]. This assessment, in turn, will allow the derivation of general conditions for DSS feasibility for hybrid testing of generic vibrating structures, thus simplifying the analysis and going well beyond the specific examples found in the current literature. It is also worth noting that actuator dynamics can be easily included in the analysis by considering the transfer function between the force F and the actuator input (e.g. voltage or current) and adding the relative degrees of such transfer function in Table 1. Similar considerations apply to potential control-structure interaction. However, such both actuator dynamics and control-structure interaction heavily depend on details of specific hardware implementation, and therefore are beyond the scope of the generic analysis presented in this paper.

Table 1. Degrees of numerators and denominators for the transfer functions described in (3) and (5).

Index i	$\angle Num_i$	$\angle Den_i$	$\angle Num1_i$	$\angle Den1_i$
n	n	2	$2n-2$	$2n$
$n-1$	$n+1$	4	$2n-3$	$2n-2$
$n-2$	$n+2$	6	$2n-4$	$2n-4$
$\vdots$	$\vdots$	$\vdots$	$\vdots$	$\vdots$
i	$2n-i$	$2n-2i+2$	$n+i-2$	$2i$
$\vdots$	$\vdots$	$\vdots$	$\vdots$	$\vdots$
1	$2n-1$	$2n$	$n-1$	2

2.2 Structural stability analysis

Structural stability plays an important role in assessing if a given system or DSS decomposition strategy will exhibit a stable and bounded dynamic response for bounded inputs. As recently shown by the authors in [36], if a polynomial with even maximum degree has only strictly positive coefficients, then it can only admit roots with negative real parts and purely imaginary roots. In this case, equation (4) can be rearranged as

$$Den_i = \prod_{q=i}^{n}(m_q s^2 + c_q s + k_q) + b_i(s) \quad i \leq n-1 \tag{7}$$

where the polynomial $b_i(s)$ includes the common factor s^2 and all of its coefficients are strictly positive. For example, given that all the parameters m_i, c_i and k_i in (4) are strictly positive, the proof shown in [36] implies that the original system only admit roots with negative real parts and hence is asymptotically stable. Although this is expected given the non-zero energy dissipation via damping, equation (7) will play a key role in assessing the structural stability of physical and numerical parts of a given DSS decomposition, as shown in Section 4.

2.3 Summary of the proposed methodology for DSS feasibility analysis

The first property that needs to be checked before designing any controller is *causality*. As defined in Section 2.1, this mathematically translates to imposing that the degree of the numerator of the input-output transfer function is less or equal to the degree of the denominator and that the region of convergence (ROC) of the Laplace transform of the impulse response is a right half plane. However, all the physical structures considered in this paper are causal by definition, therefore the ROCs of original system and of the decomposed structure always satisfy this constraint. Therefore, the causality analysis will only focus on the relative degrees of the numerators and denominators involved in the DSS controller design.

If any of the signals used in a DSS decomposition is not causal with respect to some of the inputs, then such decomposition can not be physically implemented and should be discarded. However, an alternative decomposition of the same original structure may involve only causal signals. Therefore, the first step of the methodology proposed in this paper is aimed at obtaining analytical conditions for which a given DSS decomposition involves only causal signals and can be physically implemented. An example of such analysis has been performed by Li for a specific dynamical system [38], but to the

extent of our knowledge no general analysis for generic vibration problems with an arbitrary number of degrees of freedom is present in the literature.

Once all the signals required for DSS decomposition have been proven to be causal, the next step is to check if the dynamical system to be controlled has the structural properties of *controllability* and *observability*. A system is called *controllable* if an external input can move the internal states of the system from any initial state to any other final state in a finite time interval. Similarly, a system is *observable* if its initial state can be determined based on the sequence of inputs and output signals [39]. Such structural properties are sufficient conditions to ensure that a stabilising controller can be designed[1].

A traditional result of control theory states that a linear dynamical system is controllable and observable if there are no pole-zero cancellations between the numerator and the denominator of the transfer function describing the system behaviour [40]. This analytical test will then be applied in Section 5.2 to obtain conditions under which there exists a stabilising controller capable of synchronising a given DSS decomposition.

3 DSS decomposition: types and and structural stability

Within the DSS framework, the original system shown in Figure 2 is split into two parts, a physical part implemented in hardware and a numerical part which is numerically simulated. However, different choices can be made on what subsystem should be simulated, where the interface between the two subsystems should be placed and whether force or position control should be used. Different choices give raise to different feasibility conditions, which are discussed in the rest of the paper.

For the sake of reference, in this paper the decomposition shown in Figure 3a will be called *Type 1 decomposition*, whereas the scheme shown in Figure 3b will be referred to as *Type 2 decomposition*. The difference between these two options lies in the location of the interface between numerical and physical subsystems; in Type 1 decomposition the interface is placed right after the l-th mass, whereas in Type 2 decomposition the interface is placed after the spring-damper connected to the l-th mass.

Once the location of the interface has been finalised, each part can be tested either numerically or physically. However, in Type 1 decomposition causality implies that S_1 can only be force and S_2 can only be displacement, whereas the opposite holds for Type 2 decomposition. Therefore, only four potential

---

[1]Note that observability and controllability are not necessary conditions. In fact, a stabilising controller can still be designed in presence of unobservable/uncontrollable states as long as these latter are stable. However, such weaker conditions of stabilizability and detectability can only be studied on a case by case basis, therefore they are not useful to develop the generic framework considered in this paper.
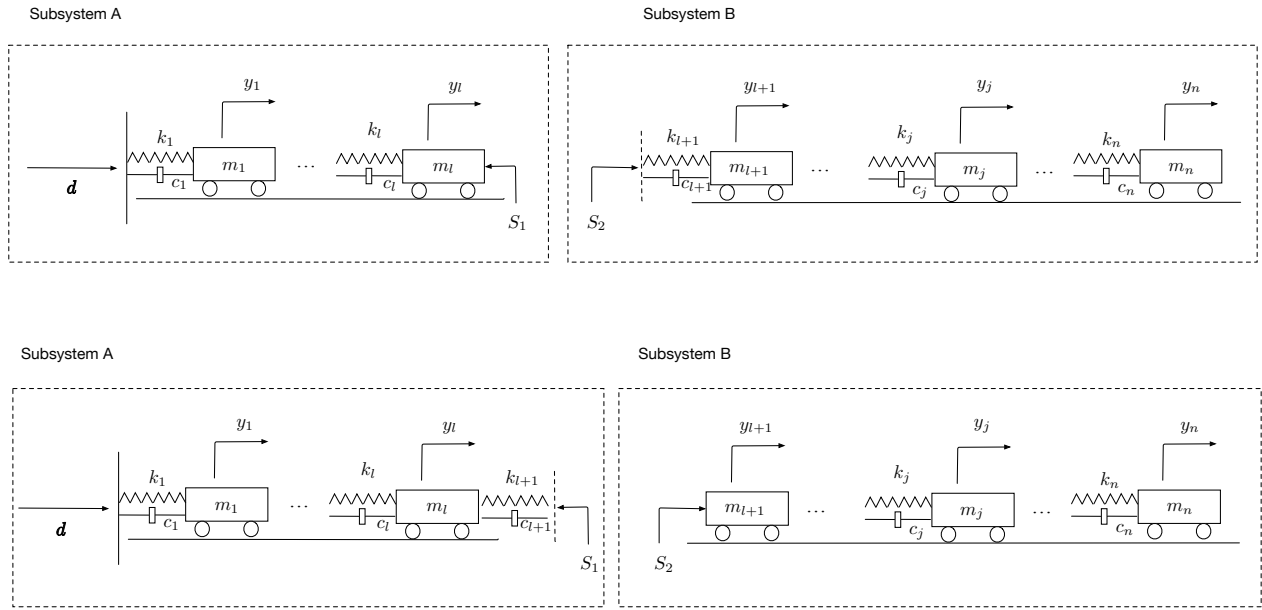
Fig. 3. Potential choices for the location of the substructuring interface: a) Type 1 decomposition where the interface is right after mass l and b) Type 2 decomposition where the interface is located after the spring-mass damper system connected to mass l.

DSS decomposition approaches will be studied in this paper.

First of all, let us note that all the subsystems in Figure 3, with the only exception of subsystem B in Type 2 decomposition, share the same structure of the original system. Therefore, their dynamics can be described by the transfer functions similar to (2) and they are all structurally stable, as expected. On the other hand, Subsystem B in Type 2 decomposition is lacking a fixed support and therefore is not asymptotically stable. Indeed, its generalised equation of motion can be derived by imposing force balance at each mass, thus obtaining

$$\frac{Y_i(s)}{F(s)} = \frac{Y_{l2}(s)}{F(s)}\frac{Y_{l+1}(s)}{y_{l2}(s)}\cdots\frac{Y_i(s)}{Y_{i-1}(s)} = \frac{Num_i^F}{Den'_{l+1}} = \begin{cases} \dfrac{Den'_{i+1}}{Den'_{l+1}} & i = l+1 \\[3mm] \dfrac{Den'_{i+1}\prod_{l+2}^{i}(c_i s + k_i)}{Den'_{l+1}} & l+2 < i \leq n-1 \\[3mm] \dfrac{\prod_{l+2}^{i}(c_i s + k_i)}{Den'_{l+1}} & i = n \end{cases} \tag{8}$$

where

$$Den'_i = \begin{cases} m_n s^2 + c_n s + k_n & i = n \\[2mm] [m_{n-1}s^2 + (c_{n-1} + c_n)s + k_{n-1} + k_n](m_n s^2 + c_n s + k_n) - (c_n s + k_n)^2 & i = n-1 \\[2mm] \vdots \\[2mm] [m_i s^2 + (c_i + c_{i+1})s + k_i + k_{i+1}]Den'_{i+1} - (c_{i+1}s + k_{i+1})^2 Den'_{i+2} & l+2 \leq i \leq n-2 \\[2mm] (m_{l+1}s^2 + c_{l+2}s + k_{l+2})Den'_{l+2} - (c_{l+2}s + k_{l+2})^2 Den'_{l+3} & i = l+1 \end{cases} \quad (9)$$

and F is the internal force applied at the interface ($F = S_2$ due to input constraint). Similar to the original system, Den'_{l+1} can be rearranged as

$$Den'_{l+1} = m_{l+1}s^2 \prod_{q=l+2}^{n}(m_q s^2 + c_q s + k_q) + b'_{l+1} \quad (10)$$

where b'_{l+1} has the common factor s^2 and its coefficients are strictly positive. Therefore, according to the approaches mentioned in Section 2.2, Den'_{l+1} can only have roots with positive real parts and two repeated roots on the origin, confirming that Subsystem B in *Type 2 decomposition* is only marginally stable. It is worth noting that in the scenario considered here, there is no fixed reference point in the physical part which can prevent drifts when the force F is applied to the $(l+1)-$th mass. Therefore, simulations are prone to drifts if the initial conditions are not known and fully consistent with the external forcing. Figure 4 shows an example of such issue, where a four-mass structure with parameters as in Table 2 is tested with a sinusoidal external physical force $F_p(t) = 3sin(6\pi t)$.

Table 2.   Numerical values of parameters used for results of Figure 4

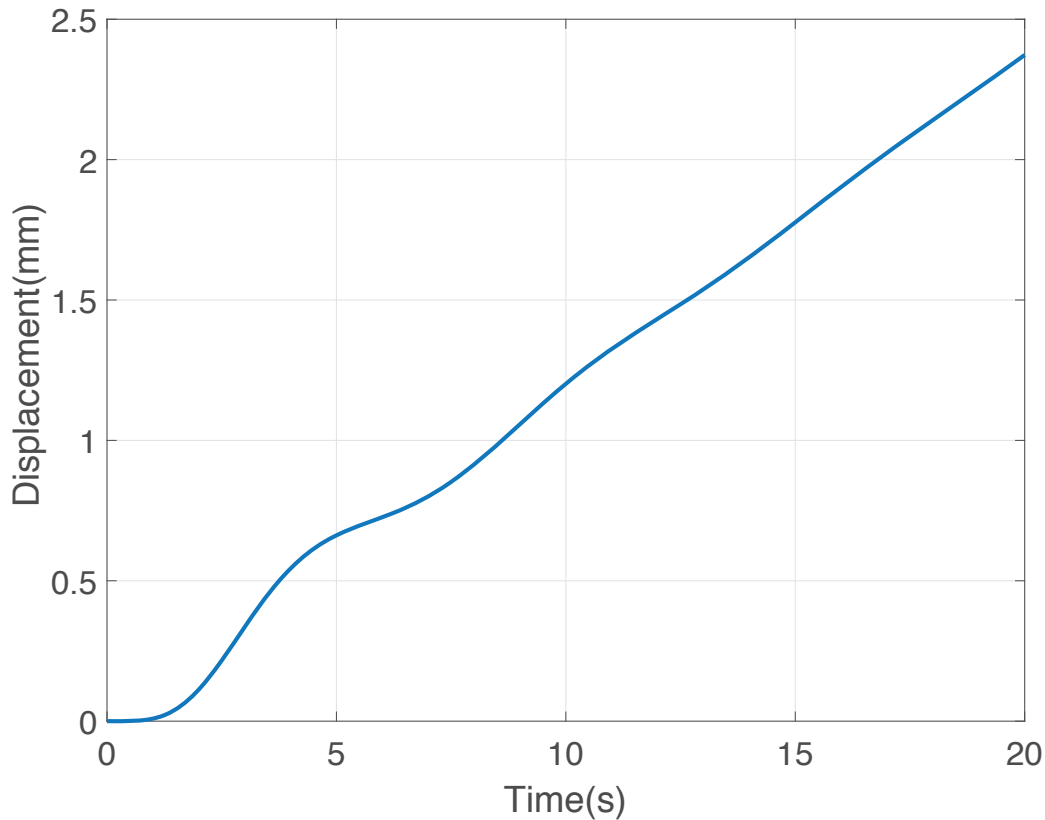| Index	Mass m_i	Stiffness k_i	Damping c_i
1	380kg	N/A	N/A
2	350kg	700N/m	250Ns/m
3	320kg	600N/m	240Ns/m
4	290kg	500N/m	230Ns/m

Fig. 4. Displacement of fourth mass with Type 2 decomposition. The drift is due to its marginal stability.

4 DSS decomposition: causality analysis

In this section, a causality analysis for all combination of substructuring types and force/position control is performed. Each feasible case is discussed in a separate subsection to improve clarity, whereas the discussion of infeasible cases is summarised in the final subsection for simplicity.

4.1 Force control, physical subsystem A, Type 1 decomposition

The general scheme for Type 1 decomposition is shown in Figure 3a and the control diagram is the same as in Figure 1. In this section we consider the case

$$S_1 = S_p = F_p, \quad S_2 = S_s = y_l, \quad S_n = F_n \tag{11}$$

i.e. the subsystem A is a physical subsystem and the physical displacement of the interface is passed to the numerical subsystem as an input. The goal of the DSS control is therefore to minimise the error between the numerical force F_n at the interface and the physical force F_p that the actuator exerts on the

physical subsystem.

The equation of motion describing mass displacements in the physical part can be written as

$$y_i = \frac{Num_i^d}{Den_d}d - \frac{Num_i^{F_p}}{Den_{F_p}}F_p \qquad\qquad 1 \leq i \leq l \qquad\qquad (12)$$

Note that equations (3)-(5) and Table 1 imply

$$\begin{aligned} \left\lfloor \frac{Num_i^d}{Den_d} \right\rfloor &= \frac{2l-i}{2l} \\ \left\lfloor \frac{Num_i^{F_p}}{Den_{F_p}} \right\rfloor &= \frac{l+i-2}{2l} \end{aligned} \qquad\qquad (13)$$

and therefore all the transfer functions related to quantities to be measured at the interface are causal[2].

Similarly, the equations of motion for the numerical subsystem read

$$\begin{aligned} y_j &= \frac{Num_j^{y_l}}{Den_{y_l}}y_l \\ &= \frac{Num_j^{y_l}}{Den_{y_l}}\left(\frac{Num_l^d}{Den_d}d - \frac{Num_l^{F_p}}{Den_{F_p}}F_p \right) \quad l+1 \leq j \leq n \end{aligned} \qquad\qquad (14)$$

Thanks to Table 1, the degree of numerators and denominators of these transfer functions can then be written as

---

[2]Note that for simplicity, all the degrees considered in this analysis are the maximum degrees and no pole-zero cancellations are taken into account. However, the same result holds even in presence of pole-zero cancellations, as the relative degree of the transfer functions is preserved also in these cases.

$$\left| \frac{Num_j^{y_l}}{Den_{y_l}} \right| = \frac{2n-j-l}{2(n-l)}$$

$$\left| \frac{Num_j^{y_l}}{Den_{y_l}} \frac{Num_i^d}{Den_d} \right| = \frac{2n-j}{2n} \tag{15}$$

$$\left| \frac{Num_j^{y_l}}{Den_{y_l}} \frac{Num_i^{F_p}}{Den_{F_p}} \right| = \frac{2n-j+l-2}{2n}$$

and therefore all the transfer functions involved in calculating mass displacements in the numerical subsystem are causal *only if* either the interface displacement y_l is passed as an input (first substitution in Equation (14)) or the combination of physical force F_p and disturbance d are passed as inputs (second substitution in Equation (14)).

On the other hand, the numerical force F_n at the interface also needs to be simulated to compute the synchronisation error fed to the DSS controller. Such numerical force can be calculated as

$$\begin{aligned}
F_n &= (c_{l+1}s+k_{l+1})(y_l-y_{l+1}) \\
&= (c_{l+1}s+k_{l+1})\left(1-\frac{Num_{l+1}^{y_l}}{Den_{y_l}}\right)y_l \\
&= (c_{l+1}s+k_{l+1})\left(1-\frac{Num_{l+1}^{y_l}}{Den_{y_l}}\right)\left(\frac{Num_l^d}{Den_d}d-\frac{Num_l^{F_p}}{Den_{F_p}}F_p\right)
\end{aligned} \tag{16}$$

Once again, Table 1 implies that the relative degrees of such transfer functions are

$$\left| (c_{l+1}s+k_{l+1})\left(1-\frac{Num_{l+1}^{y_l}}{Den_{y_l}}\right) \right| = \frac{2n-2l+1}{2(n-l)}$$

$$\left| (c_{l+1}s+k_{l+1})\left(1-\frac{Num_{l+1}^{y_l}}{Den_{y_l}}\right)\frac{Num_l^d}{Den_d} \right| = \frac{2n-l+1}{2n} \tag{17}$$

$$\left| (c_{l+1}s+k_{l+1})\left(1-\frac{Num_{l+1}^{y_l}}{Den_{y_l}}\right)\frac{Num_l^{F_p}}{Den_{F_p}} \right| = \frac{2n-1}{2n}$$

Equation (17) implies that the numerical force F_n can not be estimated in a causal way if information on y_l only is passed to the numerical subsystem. On the other hand, F_n can be obtained in a causal

way if information about F_p and d is provided, as indicated by the last substitution in Equation (16).

4.2   Position control, numerical subsystem A, Type 1 decomposition

The case analysed in this subsection refers to the same schematics shown in Section 4.1, but with the role of the physical part and the numerical part swapped, i.e.

$$S_1 = S_s = F_p, \quad S_2 = S_p = y_l^p, \quad S_n = y_l^n \tag{18}$$

The equations of motion for the physical subsystem can be written as

$$y_j = \frac{Num_j^{y_l}}{Den_{y_l}} y_l^p \qquad i+1 \le j \le n \tag{19}$$

where y_l^p is the physical displacement of the l-th mass, $Num_j^{y_l}$ and Den_{y_l} represent the numerator and the denominator of the transfer function relating input y_l^p to output y_j. According to Equation (15), all of the transfer functions are causal.

On the other hand, the equation of motion for the numerical part reads

$$y_i^n = \frac{Num_i^d}{Den_d} d - \frac{Num_i^{F_p}}{Den_{F_p}} F_p \qquad 1 \le i \le l \tag{20}$$

where y_i^n is the numerical displacement of i-th mass in subsystem A.

Due to Equation (15) all the transfer functions involved in the substructuring procedures are causal in this scenario. It is worth noting that the decomposition described in this section is feasible *only if* the physical force F_p is directly measured. In fact, if one tries to estimate it from measurements of displacements at the interface, namely

$$
\begin{aligned}
F_p &= (c_{l+1}s + k_{l+1})(y_l^p - y_{l+1}) \\
&= (c_{l+1}s + k_{l+1})\left(1 - \frac{Num_l^{y_l}}{Den_{y_l}}\right) y_l^p
\end{aligned}
\tag{21}
$$

then such an estimation is not causal.

4.3 Force control, numerical subsystem A, Type 2 decomposition

In this scenario, the original structure is decomposed as shown in Figure 3b with

$$S_1 = S_s = y_{l+1}, \quad S_2 = S_p = F_p, \quad S_n = F_n \tag{22}$$

The equation of motion for the physical part can then be written as

$$y_j = \frac{Num_j^{F_p}}{Den_{2F_p}} F_p \qquad\qquad l+1 \le j \le n \tag{23}$$

and therefore, according to Table 1,

$$\left\lfloor \frac{Num_j^{F_p}}{Den_{2F_p}} \right\rfloor = \frac{2n-j-l-1}{2(n-l)} \tag{24}$$

and the physical part is causal, as expected.

Similarly, the displacements of the masses in the numerical part can be described as

$$y_i = \frac{Num_i^d}{Den_d} d - \frac{Num_i^{y_{l+1}}}{Den_{y_{l+1}}} y_{l+1} \qquad\qquad 1 \le i \le l \tag{25}$$

which implies

$$\left\lfloor \frac{Num_i^{y_{l+1}}}{Den_{y_{l+1}}} \right\rfloor = \frac{l+i-1}{2l} \tag{26}$$

and due to Equation (13) and (26) all the displacements in the numerical part can be simulated using causal transfer functions.

On the other hand, the numerical force F_n can be expressed as

$$
\begin{aligned}
F_n &= (c_{l+1}s + k_{l+1})(y_l - y_{l+1}) \\
&= (c_{l+1}s + k_{l+1})\left[\frac{Num_l^d}{Den_d}d - \left(\frac{Num_l^{y_{l+1}}}{Den_{y_{l+1}}} + 1\right)y_{l+1}\right] \\
&= (c_{l+1}s + k_{l+1})\left[\frac{Num_l^d}{Den_d}d - \left(\frac{Num_l^{y_{l+1}}}{Den_{y_{l+1}}} + 1\right)\frac{Num_{l+1}^{F_p}}{Den_{2F_p}}F_p\right]
\end{aligned}
\tag{27}
$$

which implies

$$
\begin{aligned}
\left|(c_{l+1}s + k_{l+1})\frac{Num_l^d}{Den_d}\right| &= \frac{l+1}{2l} \\
\left|(c_{l+1}s + k_{l+1})\left(\frac{Num_l^{y_{l+1}}}{Den_{y_{l+1}}} + 1\right)\right| &= \frac{2l+1}{2l} \\
\left|(c_{l+1}s + k_{l+1})\left(\frac{Num_l^{y_{l+1}}}{Den_{y_{l+1}}} + 1\right)\frac{Num_{l+1}^{F_p}}{Den_{2F_p}}\right| &= \frac{2n-1}{2n}
\end{aligned}
\tag{28}
$$

Therefore, the numerical force F_n can not be causally estimated based on the physical displacement y_{l+1} (second line of Equation (27)). However, this causality issue can be avoided if direct measurements of the physical force F_p are available, as suggested by Equation (28).

Given that Subsystem B is marginally stable and its displacements may drift as shown in Section 3, the DSS decomposition considered in this section is dangerous to be implemented and should be avoided if possible.

4.4 Position control, physical subsystem A, Type 2 decomposition

The setup is similar to the one considered in Section 4.3, but with the role of the physical part and the numerical part swapped, i.e.

$$
S_1 = S_p = y_{l+1}^p, \quad S_2 = S_s = F_p, \quad S_n = y_{l+1}^n
\tag{29}
$$

In this case, the equation of motion for the physical part A reads

$$y_i = \frac{Num_i^d}{Den_d}d - \frac{Num_i^{y_{l+1}}}{Den_{y_{l+1}}}y_{l+1} \qquad 1 \le i \le l \tag{30}$$

and according to Equation (13) and (26), all the transfer function related to y_i are causal.

On the other hand, the physical force can be expressed as

$$
\begin{aligned}
F_p &= (c_{l+1}s + k_{l+1})(y_l - y_{l+1}) \\
&= (c_{l+1}s + k_{l+1})\left[\frac{Num_l^d}{Den_d}d - \left(\frac{Num_l^{y_{l+1}}}{Den_{y_{l+1}}} + 1\right)y_{l+1}\right]
\end{aligned}
\tag{31}
$$

Therefore, the physical force can not be estimated in a causal way from d and y_{i+1} based on Equation (28) and needs to be measured directly.

Similarly, the equations of motion describing the numerical part B read

$$y_j = \frac{Num_j^{F_p}}{Den_{2F_p}}F_p \qquad i+1 \le j \le n \tag{32}$$

Therefore, no causality problems arise as expected according to Equations (24) and (28).

4.5 Infeasible Cases

It is worth noting that for each type of decomposition, there are four possible control strategies, namely position or force control with subsystem A or subsystem B being physically tested. However, out of the eight potential strategies, only the four discussed in Sections 4.1-4.4 give raise to feasible realisations. Other cases are infeasible because, for example, the required signal can not be applied at the interface. This is the case for force control in Type 1 decomposition with subsystem A numerically simulated; the physical force F_p can not be measured or reconstructed in a causal way given that only displacement related signals are available. Similar considerations apply for: i) position control in Type 1 decomposition with subsystem B being physically tested, ii) force control in Type 2 decomposition with subsystem A being physically tested, and iii) position control in Type 2 decomposition with subsystem A being implemented numerically. A summary of feasible and infeasible cases is presented in Table 3.

4.6 Summary of Causality Analysis

The summary of the results obtained in this section is reported in Table 3, showing that only three out of four feasible decomposition strategies admit a strictly causal implementation with no potential or experimental drifts. In addition, in Type 1 decomposition, F_p can either be measured or estimated for the force control while it can only be measured for the position control. In Type 2 decomposition, F_n can only be estimated through F_p for the force control. Moreover, this strategy should be avoided if possible, due the occurrence of potential drifts in the physical part posing experimental safety issues unless when subsystem B only has single degree of freedom and a carefully tuned controller is used [41–43]. Finally, F_p can only be measured for the position control in Type 2 decomposition. Note that the analysis presented so far does not rely on detailed knowledge of the structure under test (e.g. no numerical values for the parameters are required to be known), unlike other approaches described in the literature for specific examples. This is one of the major advantages of using the recursive formulations derived in Section 2 and it simplifies the whole analysis significantly.

Table 3.   Summary of causality analysis

Control Type	Type 1	Type 2
Force Control		
(A physical)	✓	×
(A numerical)	×	✓ (Drift)
Position Control		
(A physical)	×	✓
(A numerical)	✓	×

5 DSS decomposition: structural properties

In this section the structural properties of controllability and observability of the various causal DSS decomposition strategies is derived to assess what strategies are controllable and observable, and hence admit the existence of a synchronising controller. As mentioned in Section 4, a frequency domain approach will be taken. Therefore, the analysis of structural properties reduces to obtaining conditions under which no pole-zero cancellations occur in the transfer functions used for control purposes.

5.1 Original structure structural properties

The structural properties of the original structure (before decomposition) are discussed at first in this subsection, as they form the basis for the analysis of the decomposed structure. As shown in Appendix, if the following conditions hold

$$
\begin{cases}
c_n s + k_n \perp m_n s^2 + c_n s + k_n & i = n \\
c_i s + k_i \perp m_i s^2 + (c_i + c_{i+1})s + (k_i + k_{i+1}) & i \le n-1 \\
c_{i+1} s + k_{i+1} \perp m_i s^2 + (c_i + c_{i+1})s + (k_i + k_{i+1}) & i \le n-1 \\
c_j s + k_j \perp Den_i & j = i \ldots n; \ i \le n
\end{cases}
\tag{33}
$$

then the original system is fully controllable and observable. In (33), the notation $A(s) \perp B(s)$ indicates that the polynomials $A(s)$ and $B(s)$ do not share any common root.

From a physical point of view, most of the conditions listed in Equation (33) are satisfied if none of the masses, spring or damping coefficients are zero in the original structure. Moreover, if the system is underdamped then all conditions are automatically satisfied. It is worth noting that, in any case, checking the hypotheses listed in (33) is simpler and computationally less onerous than the traditional approaches based on controllability/observability Gramians or on rank conditions on controllability matrices [39]. Indeed, testing (33) does not require neither computing all the terms in the transfer functions associated with DSS design nor a state-space representation of DSS subsystems.

5.2 Structural properties of causal DSS decompositions

Results shown in Section 5.1 can be used to analyse the structural properties of the various DSS decomposition strategies. Only strategies deemed feasible according to the analysis provided in Section 4.6 are considered here. The main focus in this section is ensuring that all the signals used by the DSS controller, and in particular the synchronisation error $e(t)$, are observable and controllable, so that the controller can effectively synchronise the two subsystems.

Let us then start with the case of force control with physical subsystem A in Type 1 decomposition.

In the numerical subsystem B, y_l plays the role of the disturbance d in the original system, therefore

$$y_{l+1} = \frac{Num_{l+1}^{y_l}}{Den_{y_l}} y_l$$

$$F_n = (c_{l+1}s + k_{l+1})(y_l - y_{l+1}) \tag{34}$$

$$= (c_{l+1}s + k_{l+1}) \left(1 - \frac{Num_{l+1}^{y_l}}{Den_{y_l}}\right) y_l$$

and the synchronisation error can be expressed as

$$e = F_p - F_n$$

$$= G_u(s)u - (c_{l+1}s + k_{l+1}) \left(1 - \frac{Num_{l+1}^{y_l}}{Den_{y_l}}\right) y_l \tag{35}$$

where $G_u(s)$ is the transfer function of the actuator (usually assumed to be a first order system). Note that all the transfer functions considered here are a subset of the transfer functions considered for the original structure and in the Appendix , therefore no pole-zero cancellations occur and the system is completely observable and controllable.

Similarly, for the case of position control with numerical subsystem A in Type 1 decomposition, the equations relative to the controller signals can be written as

$$y_l^n = \frac{Num_l^d}{Den_d} d - \frac{Num_l^{F_p}}{Den_{F_p}} F_p, \tag{36}$$

$$e = y_l^p - y_l^n = G_u(s)u - \frac{Num_l^d}{Den_d} d + \frac{Num_l^{F_p}}{Den_{F_p}} F_p \tag{37}$$

The same steps discussed in the Appendix can then be followed, yielding that the system is fully controllable and observable if

$$\begin{cases} c_l s + k_l \perp m_l s^2 + c_l s + k_l \\ c_j s + k_j \perp Den_d \qquad j = 1, \ldots, l; \end{cases} \tag{38}$$

are satisfied in addition to Equation (33). These additional constraints are introduced because the

denominator Den_d in (37) considers only the masses up to l, therefore conditions analogous to the first and the last expressions in (33) are needed.

Finally, for the case of position control with physical subsystem A in Type 2 decomposition the relevant equations read

$$
\begin{aligned}
y_{l+1}^n &= \frac{Num_{l+1}^{F_p}}{Den_{2F_p}} F_p \\
e &= y_{l+1}^p - y_{l+1}^n = G_u(s)u - \frac{Num_{l+1}^{F_p}}{Den_{2F_p}} F_p
\end{aligned}
\tag{39}
$$

Once again, such equations are a subset of the ones considered in the Appendix , therefore also this decomposition strategy is fully controllable and observable. In summary, all the causal DSS decompositions identified in Section 4 are fully controllable and observable, and therefore a synchronising controller can be successfully designed for them.

6 Numerical examples

In this section, numerical examples are discussed to highlight how the analysis performed in this paper can be used to guide the design of synchronising controllers in DSS problems. The analysis presented in this paper allows some conclusions to be drawn even before the implementation of DSS, to avoid infeasible cases as well as to predict potential difficulties during implementation. A benchmark system, falling within the class represented in Figure 2, is considered at first in Section 6.1 to show performance of the different control strategies deemed feasible via the proposed methodology. DSS control of a more complex frame structure is then analysed to show that the conclusions drawn from the analysis described in previous sections can still be used to inform feasibility by looking at, for example, the physical constraints at the interface. For the sake of clarity, detailed expressions for the controllers used in this section are reported in the Appendix.

6.1 Benchmark structure

In this section three different cases are simulated to show the control performance that can be obtained when using the DSS decompositions deemed feasible according to the analysis of Section 4 and Section 5. Detailed tuning of the controller parameters and experimental validation are beyond the scope of this paper. To perform such a numerical study, a system composed of $n = 6$ masses is

considered and the corresponding DSS decomposition is obtained by assigning three masses to the physical system and three masses to the numerical system. The numerical values of the parameters used for simulation are reported in Table 4.

Table 4.   Numerical values of parameters used for the simulation examples

Index	Mass m_i	Stiffness k_i	Damping c_i
1	500kg	1200N/m	300Ns/m
2	470kg	1100N/m	290Ns/m
3	440kg	1000N/m	280Ns/m
4	410kg	900N/m	270Ns/m
5	380kg	800N/m	260Ns/m
6	350kg	700N/m	250Ns/m

The disturbance $d(t)$ is a chirp signal of amplitude 1mm, and having a frequency increasing from 0Hz to 0.5Hz over 45s and then maintained constant for further 15s. For each case, the synchronisation controller is designed as an H_2 controller having $e(t)$ as input and using the energy of $e(t)$ as performance index to be minimised.

The results obtained for force control in Type 1 decomposition, where the physical part sits in subsystem A, are reported in Figure 5, with the physical force F_p being measured. In this case, perfect synchronisation is achieved between the numerical force F_n and the physical force F_p and the response is also close to the one exhibited by the original system.

Similarly, the results for position control in Type 1 decomposition, where the physical part now sits in subsystem B, are reported in Figure 6. Also in this case, almost perfect synchronisation is achieved, with a negligible error between physical displacement y_p and numerical displacement y_n, as well as a good match with the original response.

Finally, results for position control in Type 2 decomposition with numerical subsystem B are reported in Figure 7. In this case, synchronisation is more challenging, with some noticeable discrepancies at the local minima and maxima for the displacement. Potential reasons include a non optimal choice of poles for the closed loop system and, most importantly, the marginal stability of subsystem B causing drifts that are not compensated well by the controller. This is in accordance with the analysis in Section 4.4 where Type 2 decomposition was shown to be harder to control due to the potential drifts in the numerical part. Exact tuning of the H_2 controller to increase performance or design of more robust
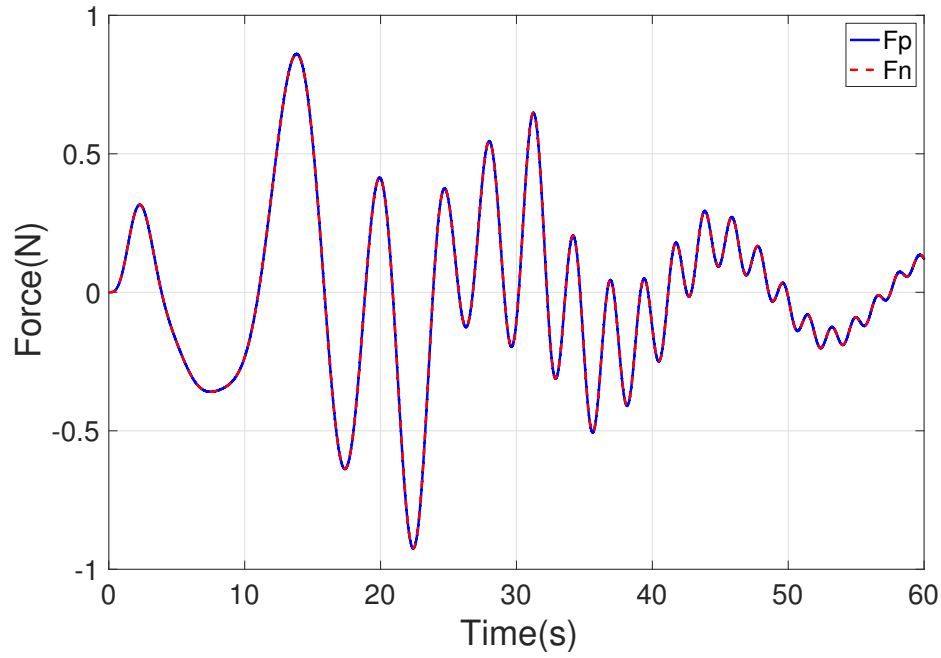
Fig. 5. Results obtained for DSS with force control in the Type 1 decomposition with physical subsystem A.
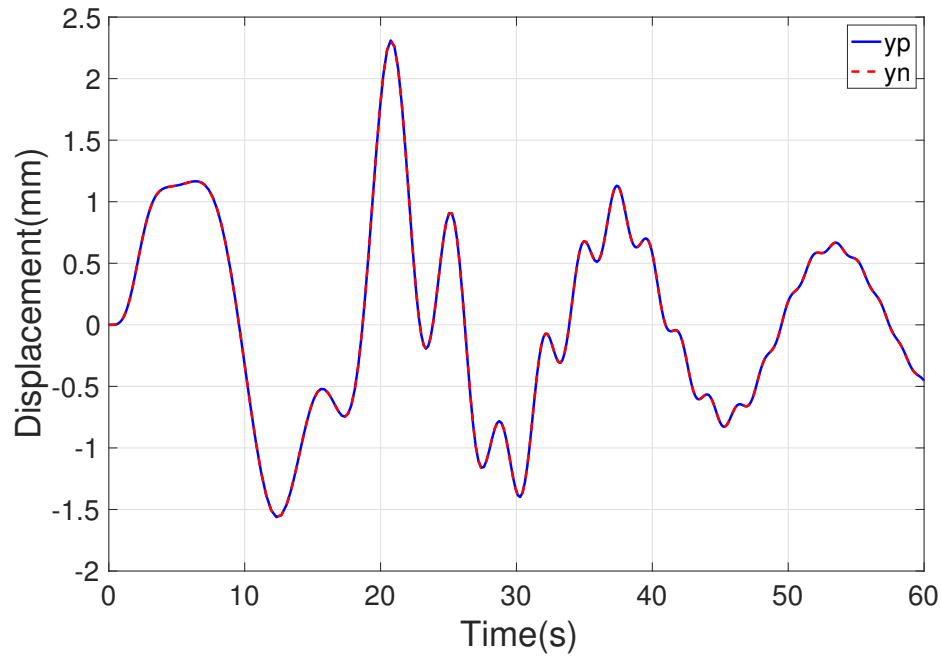

Fig. 6. Results obtained for DSS with position control in the Type 1 decomposition with numerical subsystem A.

controllers is beyond the scope of this paper. Figure 7 highlights the poorer performance obtainable with position control in Type 2 decomposition, in agreement with the advice made in the summary of causality analysis to not use this DSS decomposition strategy for real applications.
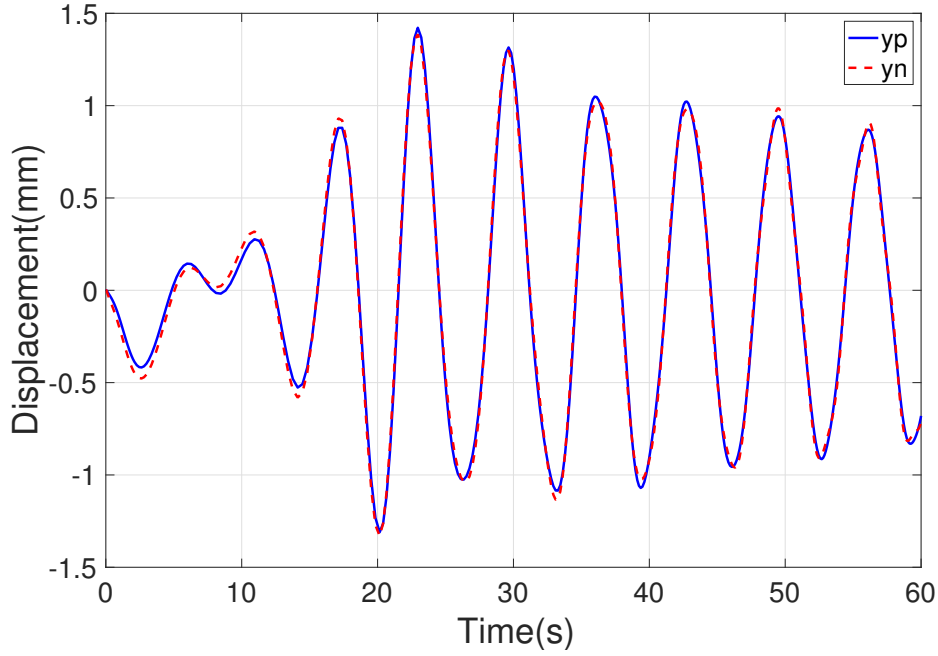
Fig. 7.   Results obtained for DSS with position control in the Type 2 decomposition with physical subsystem A.

6.2   Complex frame structure

In order to demonstrate that the analysis presented in this paper applies to generic complex structures, beyond the benchmark system illustrated in Figure 3 used to motivate the analysis, a frame structure with stronger coupling across different structural elements is considered in this section. The structure, shown in Figure 8a, is composed of several masses connected by elastic elements and may be used to model transverse oscillations in multi-storey buildings [44]. The equivalent mathematical representation of such a structure is shown in Figure 8b and its equations of motion read

$$m_4\ddot{y}_4 = -k_{34}(y_4 - y_3) - c_{34}(\dot{y}_4 - \dot{y}_3) - k_{24}(y_4 - y_2) - c_{24}(\dot{y}_4 - \dot{y}_2) \tag{40}$$

$$m_3\ddot{y}_3 = k_{34}(y_4 - y_3) + c_{34}(\dot{y}_4 - \dot{y}_3) - k_{23}(y_3 - y_2) - k_{13}(y_3 - y_1) - c_{13}(\dot{y}_3 - \dot{y}_1) \tag{41}$$

$$m_2\ddot{y}_2 = k_{24}(y_4 - y_2) + c_{24}(\dot{y}_4 - \dot{y}_2) + k_{23}(y_3 - y_2) - k_{12}(y_2 - y_1) - c_{12}(\dot{y}_2 - \dot{y}_1) \tag{42}$$

$$m_1\ddot{y}_1 = k_{13}(y_3 - y_1) + c_{13}(\dot{y}_3 - \dot{y}_1) + k_{12}(y_2 - y_1) + c_{12}(\dot{y}_2 - \dot{y}_1) - k_{11}(y_1 - d) - c_{11}(\dot{y}_1 - \dot{d}) \tag{43}$$

Numerical values of the parameters are the same as in Table 4, with k_{34}, k_{13}, k_{12} and k_{11} being set equal to k_4, k_3, k_2 and k_1, and similarly for the damping coefficients. In addition, $k_{24} = 800$N/m, $k_{23} = 500$N/m and $c_{24} = 260$Ns/m. The disturbance $d(t)$ is a $1mm$ chirp signal whose frequency increases from 0Hz to 0.7Hz over $50s$ and then is maintained constant for further 30s. Type 1 decomposition can be implemented

by placing the interface above m_1 given the similarities of the conditions at the interface: the absence of spring and damper at the interface implies that only the external force can be applied, therefore, results from Sections 4 and 5 suggest that force and position control are feasible. Indeed, it was possible to design H_2 controllers to eliminate the error between forces or displacements at the interface, in accordance with the causality and structural properties analysis. Results about force and position control are shown, respectively, in Figure 9 and 10. As expected, signals at the interface are well synchronised and the DSS responses are very close to those exhibited by the original structure. These numerical results demonstrate that the analysis discussed in this paper is valid for generic vibrating structures.
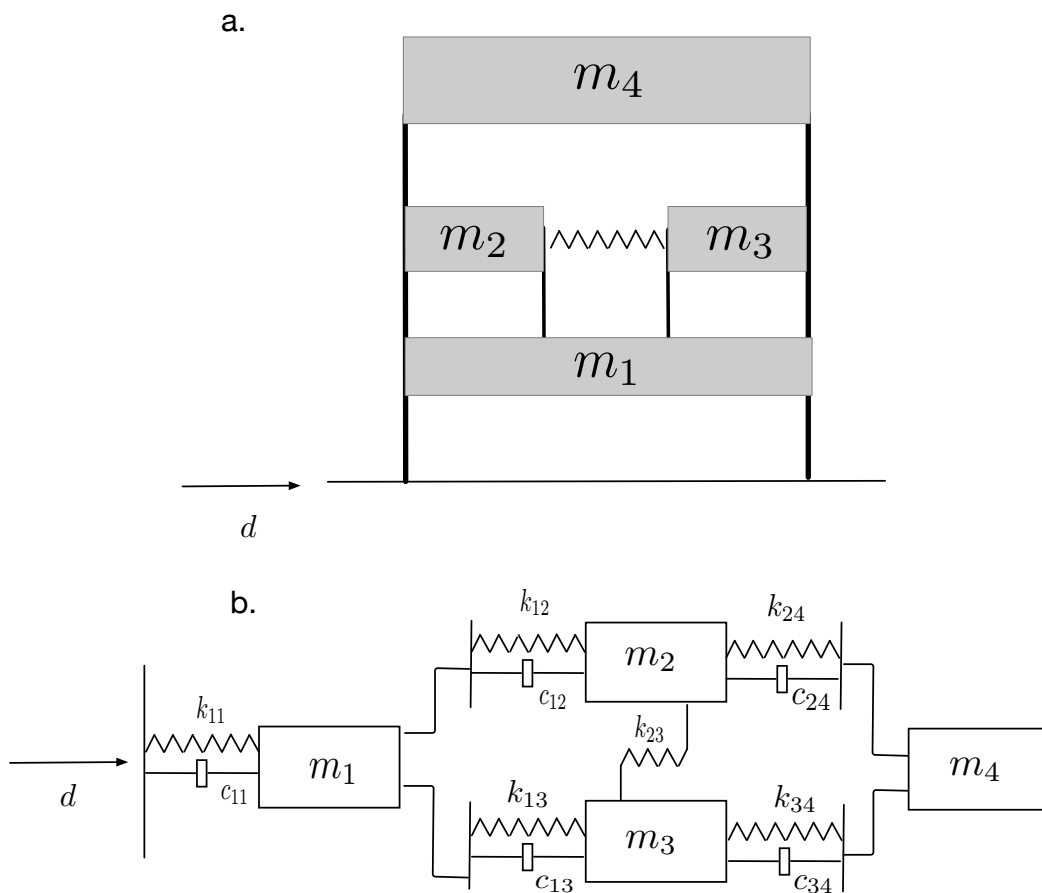
Fig. 8. Complex frame structure: a) real structure, b) equivalent mathematical representation.

7 Conclusions

A comprehensive analysis of DSS decomposition strategies for vibration problems was presented in this paper. A control-theoretic approach was explored to derive rigorous conditions for which a given
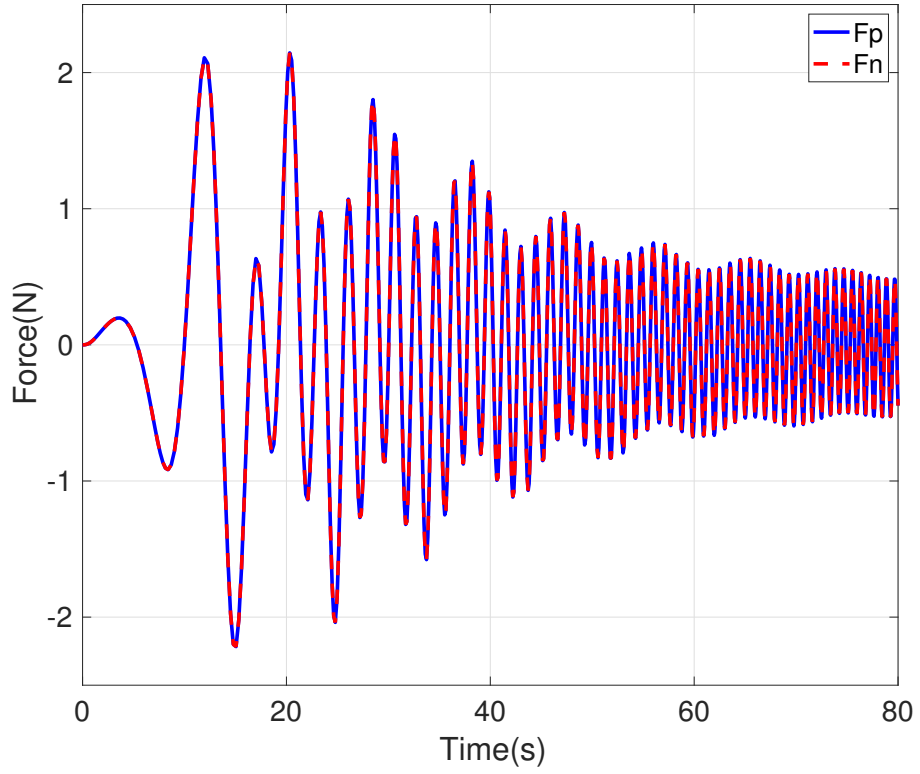
Fig. 9.   Results obtained for complex structure with force control in the Type 1 decomposition.
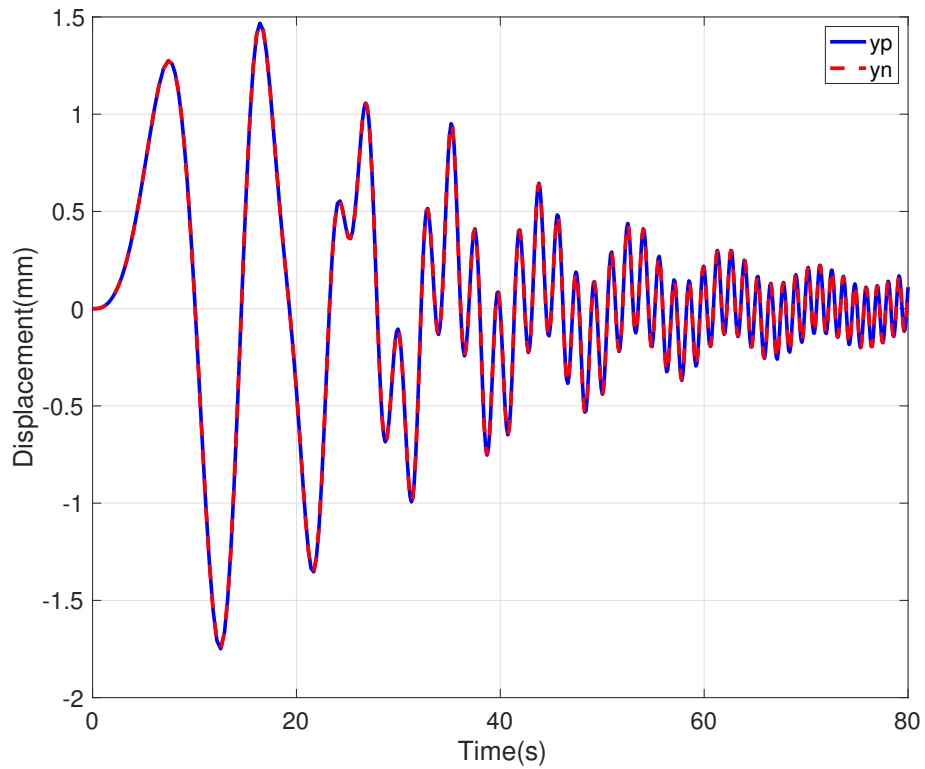

Fig. 10.   Results obtained for complex structure with position control in the Type 1 decomposition.

vibration structure can be tested within the DSS framework. The proposed method is based on a novel recursive formulation of the transfer functions involved in DSS design. The analysis presented in this paper is independent from the number of degrees of freedom present in the original structure, so it goes beyond all the specific cases described in the literature so far. Moreover, it allows feasibility analysis of DSS control for whole classes of vibrating structures, without detailed knowledge of the numerical values of their parameters. Indeed, structural stability for different sub-systems can be analysed without calculating the roots of characteristic equations and causality can be studied without knowing any of the system parameters. Moreover, the proposed methodology also provides guidelines for choosing the best DSS decomposition strategy for any given structure. Simple conditions to ensure controllability and observability of DSS design have been derived in (33) and (9). These conditions are automatically satisfied if the vibrating structure is underdamped and, in any case, can be tested with less computational effort compared to standard controllability and observability tests. The potential applicability of the results to more generic structures than the benchmark system used for the initial analysis is demonstrated on a numerical example regarding DSS control of a complex frame structure. This suggests that the proposed framework can potentially be extended to more complex structures, and investigating this problem by combining modal analysis with our framework represents a promising avenue for future work. Overall, the results presented in this paper provide rigorous guidelines for guiding the choice of DSS decomposition strategies for hybrid testing of vibrating structures.

Declaration of conflicting interests

Funding

Notation

Symbol	Definition
n	Number of masses
l	Location of DSS interface
y_i	Displacement of i-th mass
F	Force of DSS actuator
d	Disturbance acting on the system
$\angle P(s)$	Degree of polynomial $P(s)$
$\lfloor H(s) \rfloor$	Maximum degree of transfer function $H(s)$
$Num_i^{\boldsymbol{d}}$	Numerator of transfer function between $\boldsymbol{d}$ and y_i
Num_i^{d}	i-th generic numerator in subsystem A with F_p as input (Type 2 decomposition)
Den_{2F_p}	Generic denominator in subsystem B with F_p as input (Type 2 decomposition)
$Num_j^{y_l}$	j-th generic numerator in subsystem B with y_l as input (Type 1 decomposition)
Den_{y_l}	Generic denominator in subsystem B with y_l as inpu (Type 1 decomposition)
$Num_i^{y_{l+1}}$	i-th generic numerator in subsystem A with y_{l+1} as input (Type 2 decomposition)
$Den_{y_{l+1}}$	Generic denominator in subsystem A with y_{l+1} as input (Type 2 decomposition)

Appendix A: Controllability and observability of original dynamics

The complete proof of controllability and observability for the original vibrating structure discussed in Section 5.1 is reported in this appendix.

In particular, an induction procedure is used to show that under the hypotheses listed in Equation (33) there are no common roots between any denominator and numerator of the transfer functions considered in DSS design. As first step, let us note that the constraints listed in Equation (33) imply that the first two denominators Den_n and Den_{n-1} in Equation (4) do not have any common root. Let us then assume that two adjacent denominators Den_{n-i+1} and Den_{n-i} do not share any common roots. Equation (4) can be rewritten as

$$Den_{n-i-1} = K_{1(n-i-1)}Den_{n-i} - K_{2(n-i-1)}Den_{n-i+1} \tag{A.1}$$

where

$$K_{1(n-i-1)} = m_{n-i-1}s^2 + (c_{n-i} + c_{n-i})s + k_{n-i-1} + k_{n-i} \tag{A.2}$$

$$K_{2(n-i-1)} = (c_{n-i}s + k_{n-i})^2 \tag{A.3}$$

Then Equation (A.1) can be plugged into the following denominators to obtain

$$
\begin{aligned}
Den_{n-j+1} &= K_{1(n-j+1)}Den_{n-j+2} - K_{2(n-j+1)}Den_{n-j+3} \\
&= \left(\prod_{q=i+2}^{j} K_{1(n-q+1)} - b_{1(j)} \right) Den_{n-i} - \left(K_{2(n-i-1)} \prod_{q=i+3}^{j} K_{1(n-q+1)} - b_{2(j)} \right) Den_{n-i+1} \quad i+3 \leq j \leq n
\end{aligned}
\tag{A.4}
$$

where

$$K_{1(n-j+1)} = m_{n-j+1}s^2 + (c_{n-j+1} + c_{n-j+2})s + k_{n-j+1} + k_{n-j+2} \tag{A.5}$$

$$K_{2(n-j+1)} = (c_{n-j+2}s + k_{n-j+2})^2 \tag{A.6}$$

$$b_{1(i+2)} = 0 \tag{A.7}$$

$$b_{1(i+3)} = K_{2(n-i-2)} \tag{A.8}$$

$$b_{1(j)} = K_{1(n-j+1)}b_{1(j-1)} + K_{2(n-j+1)} \prod_{q=i+2}^{j-2} K_{1(n-q+1)} - K_{2(n-j+1)}b_{1(j-2)} \qquad i+4 \leq j \leq n \tag{A.9}$$

$$b_{2(i+2)} = b_{2(i+3)} = 0 \tag{A.10}$$

$$b_{2(i+4)} = K_{2(n-i-1)}K_{2(n-i-3)} \tag{A.11}$$

$$b_{2(j)} = K_{1(n-j+1)}b_{2(j-1)} + K_{2(n-j+1)}K_{2(n-i-1)} \prod_{q=i+3}^{j-2} K_{1(n-q+1)} - K_{2(n-j+1)}b_{2(j-2)} \quad i+5 \leq j \leq n \tag{A.12}$$

In the above equations, $K_{1(n-j+1)}$ and $K_{2(n-j+1)}$ are used to describe the explicit terms, while $b_{1(j)}$ and $b_{2(j)}$ are used to implicitly describe the rest of the division of Den_{n-j+1} by, respectively $K_{1(n-j+1)}$ and $K_{2(n-j+1)}$. The degrees of the polynomials $b_{1(j)}$ and $b_{2(j)}$ are reported in Table A.1 for reference.

Let us then proceed with a proof by contradiction. To this end, note that if Den_{n-j+1} and Den_{n-i-1}

Table A.1. Degrees of polynomials $b_{1(j)}$ and $b_{2(j)}$.

Index j	$\angle b_{1(j)}$	$\angle b_{2(j)}$
i+2	0	0
i+3	2	0
i+4	4	4
i+5	6	6
$\vdots$	$\vdots$	$\vdots$
j	2j-2i-4 ($j \geq i+2$)	2j-2i-4 ($j \geq i+4$)
$\vdots$	$\vdots$	$\vdots$
n	2n-2i-4	2n-2i-4

had common roots, then Equation (A.4) could be rearranged as

$$Den_{n-j+1} = A \cdot Den_{n-i-1} \tag{A.13}$$

When A is a constant or a polynomial, all roots of Den_{n-i-1} are included in the roots of Den_{n-j+1}. On the other hand, if A is a ratio of polynomials and its denominator shares some roots with Den_{n-i-1}, then some roots of Den_{n-i-1} are not included in the roots of Den_{n-j+1}. Note that Equation (A.4) can be rewritten as

$$Den_{n-j+1} = K_{1(n-i-1)} \left(\prod_{q=i+3}^{j} K_{1(n-q+1)} - \frac{b_{1(j)}}{K_{1(n-i-1)}} \right) Den_{n-i} - K_{2(n-i-1)} \left(\prod_{q=i+3}^{j} K_{1(n-q+1)} - \frac{b_{2(j)}}{K_{2(n-i-1)}} \right) Den_{n-i+1} \tag{A.14}$$

which, once combined with Equation (A.1) and Equation (A.13), implies

$$A = \prod_{q=i+3}^{j} K_{1(n-q+1)} - \frac{b_{1(j)}}{K_{1(n-i-1)}} = \prod_{q=i+3}^{j} K_{1(n-q+1)} - \frac{b_{2(j)}}{K_{2(n-i-1)}} \tag{A.15}$$

and therefore the following condition holds

$$\frac{b_{1(j)}}{K_{1(n-i-1)}} = \frac{b_{2(j)}}{K_{2(n-i-1)}} \tag{A.16}$$

It is obvious that Equation (A.16) is trivially not satisfied for $j = i+3$ due to (A.9)-(A.12). Therefore the following proof will focus on Equation (A.16) for $j > i+3$. To this end, note that given the non-zero polynomials X, Y, a_1, a_2, T, the relation

$$\frac{X}{Y} = \frac{TX + a_1}{TY + a_2} \tag{A.17}$$

holds if and only if

$$\frac{a_1}{a_2} = \frac{X}{Y} \tag{A.18}$$

Let us then rewrite Equation (A.16) as

$$\frac{b_{1(j)}}{b_{2(j)}} = \frac{K_{1(n-i-1)}}{K_{2(n-i-1)}} \tag{A.19}$$

and use Equations (A.9) and (A.12) to express $b_{1(j)}$ and $b_{2(j)}$ as

$$b_{1(j)} = TX + a_1, \qquad b_{2(j)} = TY + a_2 \tag{A.20}$$

where

$$T = K_{2(n-j+1)} \prod_{q=i+3}^{j-2} K_{1(n-q+1)} \tag{A.21}$$

$$X = K_{1(n-i-1)} \tag{A.22}$$

$$Y = K_{2(n-i-1)} \tag{A.23}$$

$$a_1 = K_{1(n-j+1)}b_{1(j-1)} - K_{2(n-j+1)}b_{1(j-2)} \tag{A.24}$$

$$a_2 = K_{1(n-j+1)}b_{2(j-1)} - K_{2(n-j+1)}b_{2(j-2)} \tag{A.25}$$

Then (A.19) holds if and only if

$$\frac{K_{1(n-j+1)}b_{1(j-1)} - K_{2(n-j+1)}b_{1(j-2)}}{K_{1(n-j+1)}b_{2(j-1)} - K_{2(n-j+1)}b_{2(j-2)}} = \frac{K_{1(n-i-1)}}{K_{2(n-i-1)}} \tag{A.26}$$

or, by rearranging the terms in a more convenient form,

$$\frac{K_{1(n-j+1)}}{K_{2(n-j+1)}} = \frac{K_{2(n-i-1)}b_{1(j-1)} - K_{1(n-i-1)}b_{2(j-1)}}{K_{2(n-i-1)}b_{1(j-2)} - K_{1(n-i-1)}b_{2(j-2)}} \tag{A.27}$$

However, according to (A.5)-(A.6) and Table A.1, the left hand side is a ratio of second order polynomials, whereas the right hand side is a ratio of polynomials of different degrees. Therefore (A.27) can not hold and the proof is concluded, indicating that in the original structure no common roots exist between Num_i and Den_i $(1 \leq i \leq n)$ if the hypotheses listed in (33) hold. The original system is then fully controllable and observable.

Appendix B: H_2 controllers used for numerical results shown in the main paper

For the sake of completeness, explicit numerical expressions for the controllers designed in Section 6 are reported in this appendix. Controller for Type 1 decomposition with force control in the benchmark system, used to obtain results shown in Figure 5:

$$C(s) = \frac{2.9306 \times 10^6 (s+10)(s+3.781)(s+3.589)(s+3.328)(s^2+0.002372s+2.681 \times 10^{-6})}{(s+1.003 \times 10^5)(s^2+0.006758s+0.1492)(s^2+0.3164s+1.124)(s^2+0.8353s+2.843)} \times$$

$$\times \frac{(s^2+0.6761s+1.979)(s^2+2.014s+5.917)(s^2+132s+8950)}{(s^2+1.399s+4.581)(s^2+2.037s+6.571)(s^2+2.339s+8.129)} \tag{B.1}$$

Controller for Type 1 decomposition with position control in the benchmark system, used to obtain results shown in Figure 6:

$$C(s) = \frac{-2.6375 \times 10^{10}(s+65.33)(s+10)(s+3.793)(s+3.571)(s^2+0.1433s+0.4533)}{(s+10^9)(s^2+0.4257s+0.4533)(s^2+0.3281s+1.093)(s^2+0.8342s+2.758)} \times$$

$$\times \frac{(s^2+1.048s+3.141)(s^2+2.158s+6.492)(s^2+62.11s+5636)}{(s^2+1.446s+4.779)(s^2+2.029s+6.688)(s^2+2.312s+7.938)} \tag{B.2}$$

Controller for Type 2 decomposition with position control in the benchmark system, used to obtain results shown in Figure 7:

$$C(s) = \frac{1.2628 \times 10^{13}(s+1.173)(s+10)(s^2+0.145s+0.4791)(s^2+1.038s+3.103)}{(s+9.872 \times 10^7)(s+1.279 \times 10^6)(s+2.814)(s^2+0.4184s+0.6607)(s^2+0.02365s+0.908)} \times$$

$$\times \frac{(s^2+3.205s+5.738)(s^2+2.172s+6.498)(s^2+1.087s+12.08)}{(s^2+1.119s+3.217)(s^2+2.196s+6.525)(s^2+1.621s+6.191)} \tag{B.3}$$

Controller for Type 1 decomposition with force control in the complex frame system, used to obtain results shown in Figure 9:

$$C(s) = \frac{1.4101 \times 10^6(s+3.684)(s^2+0.002657s+1.534 \times 10^{-5})(s^2+1.856s+6.01)(s^2+1.231s+6.374)}{(s^2+0.1155s+0.4773)(s^2+1.517s+5.154)(s^2+1.224s+6.405)(s^2+2.593s+9.28)} \tag{B.4}$$

Controller for Type 1 decomposition with position control in the complex frame system, used to obtain

results shown in Figure 10:

$$C(s) = \frac{2.2243 \times 10^{12}(s+1.112 \times 10^4)(s+20)(s^2+0.3835s+1.377)(s^2+2.112s+6.961)(s^2+1.218s+6.357)}{(s+2 \times 10^9)(s^2+0.1242s+0.4791)(s^2+1.516s+5.15)(s^2+1.224s+6.405)(s^2+2.589s+9.246)}$$

(B.5)

References

[1] Chen, C., Ricles, J. M., Marullo, T. M., and Mercan, O., 2009. "Real-time hybrid testing using the unconditionally stable explicit cr integration algorithm". *Earthquake Engineering & Structural Dynamics,* **38**(1), pp. 23–44.

[2] Mosterman, P. J., 1999. "An overview of hybrid simulation phenomena and their support by simulation packages". In International Workshop on Hybrid Systems: Computation and Control, Springer, pp. 165–177.

[3] Maghareh, A., Dyke, S. J., Prakash, A., and Bunting, G. B., 2014. "Establishing a predictive performance indicator for real-time hybrid simulation". *Earthquake engineering & structural dynamics,* **43**(15), pp. 2299–2318.

[4] Tu, J. Y., 2013. "Development of numerical-substructure-based and output-based substructuring controllers". *Structural Control and Health Monitoring,* **20**(6), pp. 918–936.

[5] Klerk, D. D., Rixen, D. J., and Voormeeren, S. N., 2008. "General framework for dynamic substructuring: History, review and classification of techniques". *AIAA Journal,* **46**(5), May, pp. 1169–1181.

[6] Lim, C. N., Neild, S. A., Stoten, D. P., Drury, D., and Taylor, C. A., 2007. "Adaptive control strategy for dynamic substructuring tests". *Journal of Engineering Mechanics,* **133**(8), pp. 864–873.

[7] Gawthrop, P., Wallace, M., Neild, S., and Wagg, D., 2007. "Robust real-time substructuring techniques for under-damped systems". *Structural Control and Health Monitoring,* **14**(4), pp. 591–608.

[8] Tu, J.-Y., Chen, C.-Y., and Hsiao, W.-D., 2015. "Dynamic and numerical issues relating to the control robustness of dynamically substructured systems". *Structural Control and Health Monitoring,* **22**(3), pp. 518–534.

[9] Yamaguchi, T., and Stoten, D. P., 2016. "Synthesised H_∞ / μ control design for dynamically substructured systems". *Journal of Physics: Conference Series,* **744**(1), p. 012205.

[10] Wu, B., and Zhou, H., 2014. "Sliding mode for equivalent force control in real-time substructure testing". *Structural Control and Health Monitoring,* **21**, pp. 1284–1303.

[11] Wu, B., and Wang, T., 2014. "Model updating with constrained unscented Kalman filter for hybrid

testing". *Smart Structures and Systems,* **14**(6), pp. 1105–1129.

[12] Carrion, J. E., and B.F. Spencer, J., 2008. "Real-time hybrid testing using model-based delay compensation". *Smart Structures and Systems,* **4**(6), pp. 809–828.

[13] Liu, J., Dyke, S. J., Liu, H.-J., Gao, X.-Y., and Phillips, B., 2013. "A novel integrated compensation method for actuator dynamics in real-time hybrid structural testing". *Structural Control and Health Monitoring,* **20**(7), pp. 1057–1080.

[14] Shi, P., Wu, B., Spencer Jr., B. F., Phillips, B. M., and Chang, C.-M., 2016. "Real-time hybrid testing with equivalent force control method incorporating Kalman filter". *Structural Control and Health Monitoring,* **23**(4), pp. 735–748.

[15] Maghareh, A., Dyke, S., Rabieniaharatbar, S., and Prakash, A., 2017. "Predictive stability indicator: a novel approach to configuring a real-time hybrid simulation". *Earthquake Engineering & Structural Dynamics,* **46**(1), pp. 95–116.

[16] Botelho, R. M., Gao, X., Avci, M., and Christenson, R., 2022. "A robust stability and performance analysis method for multi-actuator real-time hybrid simulation". *Structural Control and Health Monitoring,* **29**(10), p. e3017.

[17] Enokida, R., and Kajiwara, K., 2019. "Nonlinear signal-based control for single-axis shake tables supporting nonlinear structural systems". *Structural Control and Health Monitoring*, p. e2376.

[18] Drazin, P. L., and Govindjee, S., 2017. "Hybrid simulation theory for a classical nonlinear dynamical system". *Journal of Sound and Vibration,* **392**, pp. 240 – 259.

[19] Stoten, D. P., Yamaguchi, T., and Yamashita, Y., 2016. "Dynamically substructured system testing for railway vehicle pantographs". *Journal of Physics: Conference Series,* **744**(1), p. 012204.

[20] Facchinetti, A., and Bruni, S., 2012. "Hardware-in-the-loop hybrid simulation of pantograph–catenary interaction". *Journal of Sound and Vibration,* **331**(12), pp. 2783–2797.

[21] Hong, W., Kang, S., Lee, J.-S., Byun, Y., and Choi, C., 2016. "Characterization of railroad track substructures using dynamic and static cone penetrometer". In Proceedings of the 5th International Conference on Geotechnical and Geophysical Site Characterisation, ISC 2016, Vol. 1, Australian Geomechanics Society, pp. 707–710.

[22] Allen, M. S., and Mayes, R. L., 2018. "Recent advances to estimation of fixed-interface modal models using dynamic substructuring". In *Dynamics of Coupled Structures, Volume 4*. Springer, pp. 157–170.

[23] Mayes, R. L., and Arviso, M., 2010. "Design studies for the transmission simulator method of experimental dynamic substructuring". In ISMA2010 International Conference on Noise and Vibration

Engineering, ISMA2010 International Conference on Noise and Vibration Engineering.

[24] van der Seijs, M., and Rixen, D., 2016. "Experimental dynamic substructuring: analysis and design strategies for vehicle development". PhD thesis, Delft University of Technology, Delft.

[25] Stoten, D. P., and Hyde, R. A., 2006. "Adaptive control of dynamically substructured systems: The single-input single-output case". *Proceedings of the Institution of Mechanical Engineers, Part I: Journal of Systems and Control Engineering,* **220**(2), pp. 63–79.

[26] Zapateiro, M., Karimi, H. R., Luo, N., and Spencer Jr, B. F., 2010. "Real-time hybrid testing of semiactive control strategies for vibration reduction in a structure with MR damper". *Structural Control and Health Monitoring,* **17**(4), pp. 427–451.

[27] Chu, S.-Y., Lu, L.-Y., and Yeh, S.-W., 2018. "Real-time hybrid testing of a structure with a piezo-electric friction controllable mass damper by using a shake table". *Structural Control and Health Monitoring,* **25**(3), p. e2124.

[28] Zhu, F., Wang, J.-T., Jin, F., Lu, L.-Q., Gui, Y., and Zhou, M.-X., 2017. "Real-time hybrid simulation of the size effect of tuned liquid dampers". *Structural Control and Health Monitoring,* **24**(9), p. e1962.

[29] Mercan, O., Ricles, J., Sause, R., and Marullo, T., 2008. "Real-time large-scale hybrid testing for seismic performance evaluation of smart structures". *Smart Structures and Systems,* **4**(5), pp. 667–684.

[30] Londoño, J. M., Serino, G., Wagg, D. J., Neild, S. A., and Crewe, A. J., 2012. "On the assessment of passive devices for structural control via real-time dynamic substructuring". *Structural Control and Health Monitoring,* **19**(8), pp. 701–722.

[31] Fu, B., Jiang, H., and Wu, T., 2019. "Experimental study of seismic response reduction effects of particle damper using substructure shake table testing method". *Structural Control and Health Monitoring,* **26**(2), p. e2295.

[32] Bursi, O. S., Abbiati, G., and Reza, M. S., 2014. "A novel hybrid testing approach for piping systems of industrial plants". *Smart Structures and Systems,* **14**(6), pp. 1005–1030.

[33] Guo, J., Tang, Z., Chen, S., and Li, Z., 2016. "Control strategy for the substructuring testing systems to simulate soil-structure interaction". *Smart Structures and Systems,* **18**(6), pp. 1169–1188.

[34] Terkovics, N., Neild, S., Lowenberg, M., Szalai, R., and Krauskopf, B., 2016. "Substructurability: the effect of interface location on a real-time dynamic substructuring test". *Proc. R. Soc. A,* **472**(2192), p. 20160433.

[35] Gawthrop, P., Neild, S., Gonzalez-Buelga, A., and Wagg, D., 2009. "Causality in real-time dynamic substructure testing". *Mechatronics,* **19**(7), pp. 1105–1115.

[36] Hu, A., and Paoletti, P., 2020. "A novel control architecture for marginally stable dynamically substructured systems". *Mechanical Systems and Signal Processing,* **143**, p. 106834.

[37] Oppenheim, A., Willsky, A., Nawab, H., and Hamid, S., 1998. *Signals and Systems*. Pearson Education.

[38] Li, G., 2014. "Dynamically substructured system frameworks with strict separation of numerical and physical components". *Structural Control and Health Monitoring,* **21**(10), pp. 1316–1333.

[39] Kalman, R., 1959. "On the general theory of control systems". *IRE Transactions on Automatic Control,* **4**(3), December, pp. 110–110.

[40] Antsaklis, P., and Michel, A., 2007. *A Linear Systems Primer*. Birkhäuser.

[41] Neild, S., Stoten, D., Drury, D., and Wagg, D., 2005. "Control issues relating to real-time substructuring experiments using a shaking table". *Earthquake engineering & structural dynamics,* **34**(9), pp. 1171–1192.

[42] Tu, J.-Y., Hsiao, W.-D., and Chen, C.-Y., 2014. "Modelling and control issues of dynamically substructured systems: adaptive forward prediction taken as an example". *Proc. R. Soc. A,* **470**(2168), p. 20130773.

[43] Barton, D. A., 2017. "Control-based continuation: Bifurcation and stability analysis for physical experiments". *Mechanical Systems and Signal Processing,* **84**, pp. 54–64.

[44] Del Carpio Ramos, M., Mosqueda, G., and Hashemi, M. J., 2016. "Large-scale hybrid simulation of a steel moment frame building structure through collapse". *Journal of Structural Engineering,* **142**(1), p. 04015086.

List of Figures

List of Tables